Atlas of Ocean Tidal Charts and Maps, Part I: The Semidiurnal Principal Lunar Tide M_2

Ernst W. Schwiderski

U.S. Naval Surface Weapons Center
Dahlgren, Virginia 22448

Abstract In this paper the author presents the NSWC ocean tide model of the semidiurnal principal lunar (M_2) tide in an atlas of ocean tidal charts and maps. The model is the computer result of a unique combination of mathematical and empirical techniques, which was introduced, extensively tested, and evaluated by Schwiderski (1978a, 1980a, b, 1983e). The computed M_2 amplitudes and phases are tabulated along with all specially labeled empirical input data on a 1° × 1° grid system in 42° × 71° overlapping charts covering the whole oceanic globe. Corresponding global and arctic corange and cotidal maps are included to provide a quick overview of the major tidal phenomena. Significant qualitative and quantitative features are explained and discussed for proper application. In particular, the charted harmonic constants may be used to compute instantaneous M_2 ocean tides with an accuracy of better than 5 cm any time and anywhere in the open oceans. Limitations of this accuracy in coastal waters and border seas are mentioned.

The following four sections of this paper deal with brief reviews, detailed evaluations, and simple improvements of general

Marine Geodesy, Volume 6, Number 3-4
0149-0419/83/020219-00$02.00/0

and special applications of the NSWC ocean tide model. In spite of the numerous and diverse applications with potential possibilities of erroneous interpretations, the results are gratifying without exceptions. For instance, it is concluded that the computed low-degree spherical harmonic coefficients of the M_2 ocean tide model agree with recent empirical satellite solutions as closely as one could wish for within the elaborated nonmodel error bounds. Detailed computations of all significant tidal energy terms produced the following noteworthy results: The rate of supplied tidal energy of $3.50Z10^{12}$ Watt matches Cartwright's (1977) estimate of $3.5Z10^{12}$ Watt. The rate of energy loss by bottom friction and displacement over the shelves is $1.50Z10^{12}$ Watt, which fits into Miller's (1966) estimated range of $(1.4–1.7)Z10^{12}$ Watt, with a clear bias toward his preferred lower bound. Perhaps most remarkably, the computed range $(0.41–0.60)Z10^{12}$ Watt for the rate of deep bottom friction work done by the unresolved fluctuating (internal or baroclinic) currents contains in its center Munk's (1966) estimate of $0.5Z10^{12}$ Watt and lies safely below Wunsch's (1975) extreme upper bound of $0.7Z10^{12}$ Watt, which both authors derived for the rate of energy needed to sustain the internal tidal circulations. As is commonly believed, the results substantiate the fact that the total rate of ocean eddy dissipation (into heat) by the averaged (surface or barotropic) currents and their fluctuating comotions is negligible within three significant figures. Finally, the total tidal energy budget of the oceans is perfectly balanced in realistic terms. Budget deficits in earlier tide models were traced to the following tacit assumptions: The ocean bottom tide is doing positive work on the oceans against the ocean tide. In fact, the bottom displacement work by the ocean tide against the bottom tide is an energy loss at the rate of $1.64Z10^{12}$ Watt. The transfer of G. I. Taylor's quadratic bottom friction term from the Irish Sea to the global oceans without accounting for major differences in area resolution scales is directly responsible for significant budget deficits in semiempirical estimates. In contrast, the hydrodynamically more consistent and realistic linear law of bottom friction encountered no serious transplantation difficulties.

The NSWC Ocean Tide Model

Schwiderski (1978a, 1980a, b, 1983e) introduced and extensively tested a unique combination of mathematical and empirical tech-

niques to compute harmonic partial tides in the realistic world oceans in great detail and with a combined tide prediction accuracy of better than 10 cm. The novel technique was first applied to construct the dominant semidiurnal principal lunar (M_2) tide with a prediction accuracy of better than 5 cm any time and anywhere in the open oceans. The M_2 model and its achieved accuracy were further evaluated and discussed in subsequent publications and presentations by the author (Schwiderski 1978b, 1979a, b, c, 1980c, 1981b).

The estimated accuracy of the constructed M_2 model was based on the worldwide smooth agreement of the computed tidal constants with empirical tidal data regardless of whether they were hydrodynamically interpolated or excluded. After the construction of the first M_2 tide model, the author received in private communications numerous new or improved empirical ocean tide data from Gill and Porter (1978, from deep-sea stations in the New York Bight), Wyrtki (1978, from island stations in the Pacific Ocean), Zetler (1978, from deep-sea and shore stations in the southeastern Indian Ocean; see Irish and Snodgrass 1972), and Cartwright (1979, from 108 deep-sea stations in the North Atlantic, northeastern Pacific, and southeastern Indian Oceans; see Cartwright et al., 1979). In addition, in early 1979 the author received the entire (3,898 stations) worldwide ocean tide data collection of the International Hydrographic Bureau (1978), which was updated and taped by the Canadian Marine Environmental Data Service.

With few exceptions of apparently erratic tabulations, the empirical data from all those sources substantiated everywhere the estimated enormous accuracy of the tide model. For example, the deep-sea profile measurements of tides in the New York Bight by Gill and Porter (1980) verified the globally modeled, incredibly sharp tide decay (Figures 1 and 2) across the continental shelf of less than 200-km width from a range (= double amplitude) of 4.6 ft at the coast to an almost constant range of 3 ft in the deep ocean (see Table 4A in Schwiderski, 1980b, and the new, slightly improved Tables 8M or 8N in Appendix A, which include the Gill and Porter data in interpolated form as indicated by subbrackets).

For the novel hydrodynamical interpolation technique, it was emphasized in Schwiderski (1978a, 1980b, c) that hydrodynami-

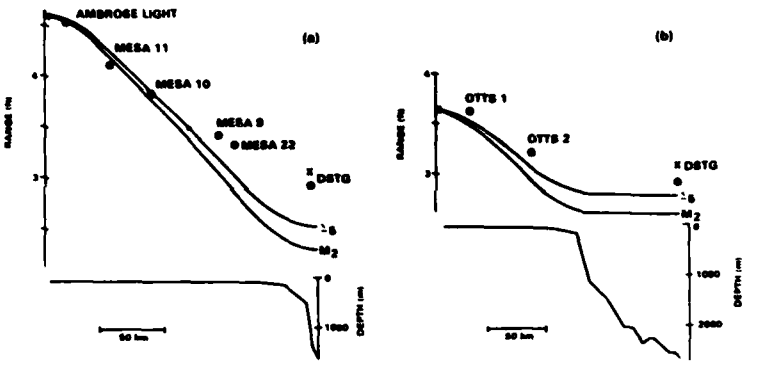

Figures (1) and (2). Gill and Porter (1980) Measurements of decaying tidal ranges across continental shelf of New York Bight: (1) Southeast of Sandy Hook, New Jersey; (2) southeast of Bethany Beach, Delaware.

M_2 = Defant shelf model, Σ_2 = Gill-Porter Shelf Model, x = Schwiderski (1978a) Global Model

cally interpolated marginal empirical tide data in isolated grid cells distort the surrounding computed ocean tide only insignificantly. This fortunate feature has been established by extensive computer experiments and is illustrated here by the following interesting example. In Table 5B in Schwiderski, 1980b, one finds in the grid cell M = 236 and N = 52 the obviously somewhat incoherent phase value $\delta = 227°$. This near-shore, deep-sea empirical datum (marked by a subbracket) was taken from publications by Irish et al. (1971), Nowroozi (1972), and others, and was hydrodynamically interpolated into the tide model. The slightly anomalous datum was well noticed but retained as a possible retardation result of the nearby San Francisco Bay entrance and the proximity of the Farallon Islands.

However, in 1979 Cartwright (see revised insert in Cartwright et al., 1979) communicated to the author the more plausible and correct phase value $\delta = 206°$, which he derived from the earlier original publication by Nowroozi et al. (1969). Evidently the correct datum fits coherently into Table 5B in Schwiderski, 1980b (where the erroneous value is interpolated) and into the new tables

(6M or 6N) in Appendix A, where the correct value is interpolated. Naturally, it was mentioned in Schwiderski (1978a, 1980b, c) that the accuracy of the constructed tidal charts depends to some degree on the quality and quantity of the hydrodynamically interpolated data. After the arrival of the numerous and improved empirical data collections mentioned above, the author found it justified to improve the original M_2 ocean tide by additional computations with revised empirical data inputs.

In particular, the new data included slightly enhanced tidal amplitudes around the British Isles where earlier computations had to depend on marginal older data collections (Schwiderski 1978a, 1980b), because the tide tables of the British Admiralty (1977) listed no harmonic constants for the European waters. The new tape of tidal constants collected by the International Hydrographic Bureau (1978) filled this undesirable gap. Moreover, most of the numerous deep-sea tide data compiled by Cartwright (Cartwright et al., 1979) around the British Isles qualified as near-shore data and could be hydrodynamically interpolated into the new model (Schwiderski 1978a, 1980b, c). Similarly, the deep-sea tide data determined by the Canadian Hydrographic Service (Cartwright et al., 1979) for stations south of the Bay of Fundy between Nova Scotia and Cape Cod could be interpolated as near-shore data, which led to slightly lower amplitudes.

Finally, it must be mentioned that the phase data in the tide tables of the British Admiralty (1977) and on the tape of the International Hydrographic Bureau (1978) differ by as much as 30° for the northwestern coast of India. Apparently, these unwanted differences can be traced to different interpretations of the time origin in both listings. After a telephone conversation with Mr. P. A. Bolduc of the Canadian Marine Environmental Data Service, who supervised the taping and revision of the data of the International Hydrographic Bureau, the data used earlier from the British Admiralty were slightly revised. Subsequent computations indicated that the new phases seem to fit the general tide behavior in that area (e.g., Laccadiven tide data; Table 2M) somewhat better.

Along with the revised empirical input data, the reconstruction of the M_2 tide included also a new higher order approximation of

Arctic Ocean tides, which is described in Schwiderski (1983e). The novel expansion improved the original M_2 model near the North Pole by about 6 cm in amplitudes. This improvement faded quickly southward and vanished below 17° colatitude.

In the following section, "Parameters of M_2 Ocean Tide Model," one finds all mode-dependent hydrodynamical input parameters that specified the reconstructed M_2 ocean tide. In the subsequent section, "M_2 Ocean Tide Features," quantitative and qualitative features of the M_2 ocean tide are pointed out and discussed.

A complete listing of all sources of empirical ocean tide data, which were interpolated into the new, slightly improved M_2 tidal charts, is presented in "Acknowledgments." A complete $1° \times 1°$ numerical display of the M_2 model is presented in Appendix A, where all tidal amplitudes and phases are tabulated gridwise in maplike charts. Corange and cotidal maps of the M_2 ocean tide are plotted in Appendix B.

The present NSWC Ocean Tide Model (Schwiderski, 1981a) now includes similar charts of the leading semidiurnal (M_2, S_2, N_2, K_2), diurnal (k_1, O_1, P_1, Q_1), and long-period (Mf, Mm, Ssa) harmonic partial tides (see Tables 1 and 10). The major relative features of all eleven constituents will be discussed in Schwiderski, 1983d. The harmonic constants of all 11 partial tides are listed on the NSWC Global Ocean Tide (GOTD 1981) Tape (Schwiderski, 1981a), which is described in Schwiderski and Szeto (1981a).

The wide-ranging subject of applications of ocean tides goes far beyond the original scope of this paper, which was set by this journal's editor on recommendations of his earlier referees who refereed the author's preceding papers (Schwiderski 1980a, b). As requested, the original paper presented only the complete results of the author's M_2 ocean tide model, which was fully described, analyzed, and reviewed in contrast to other well-known tide models (such as Pekeris and Accad, 1969; Zahel, 1970, 1977; Hendershott, 1972; Marchuk et al., 1973; Marchuk and Kagan, 1977; Estes, 1977, 1980; Accad and Pekeris, 1978; Parke and Hendershott, 1980; and many more) in Schwiderski, 1980a, b, c. Stimulated by some comments of one of the present referees, the author decided to add four sections on various applications and simple

Table 1
Leading harmonic equilibrium tides.

Tidal Mode		*Period*	*Amplitude*[a]
	Semidiurnal Species		
M_2:	Principal Lunar	12.421 h	100.000%
S_2:	Principal Solar	12.000 h	46.564%
N_2:	Elliptical Lunar	12.568 h	19.146%
K_2:	Declination Luni-Solar	11.967 h	12.670%
	Diurnal Species		
K_1:	Declination Luni-Solar	23.935 h	58.417%
O_1:	Principal Lunar	25.819 h	41.502%
P_1:	Principal Solar	24.066 h	19.330%
Q_1:	Elliptical Lunar	26.868 h	7.946%
	Long-Period Species		
Mf:	Fortnightly Lunar	13.661 d	17.225%
Mm:	Monthly Lunar	27.555 d	9.089%
Ssa:	Semiannual Solar	182.621 d	8.024%

[a] Amplitudes relative to M_2 equilibrium amplitude (K = 24.2334 cm). All neglected minor partial tides have amplitudes less than 4% of the M_2 amplitude K. (See also Table 10.)

improvements of his completed eleven-mode ocean tide model in general and of his M_2 model in particular. Though most of these ongoing applications are still in a premature state of the art, this reviewing addition was considered necessary because the extraordinary broad range and involved complexity of the investigated problems naturally carry with them the potential for improper or erroneous interpretation or use of the assumed tide model.

Parameters of M_2 Ocean Tide Model

The following M_2 ocean tide parameters (see also Table 10) are needed in applications of the harmonic constants tabulated in the charts of Appendix A or on the NSWC GOTD 1981 Tape (Schwiderski and Szeto, 1981a).

The astronomical semidiurnal principal lunar (M_2) equilibrium tide η (or tide-generating potential $G\eta$; see Schwiderski 1978a, 1980a) at the geographical point (λ, ϕ) and instant (Y, D, t) is determined by

$$\eta = K \cos^2 \phi \cos(\alpha t + \chi + 2\lambda) \qquad (1)$$

where

G = 9.81 m/sec^2 earth gravity acceleration
λ = longitude (east in rad)
ϕ = latitude (north in rad)
Y ($\geq$ 1975) = year number
D = day number of year Y(D = 1 for January 1)
t = universal standard time of day D (in sec)
K = 0.242 334 m = M_2 equilibrium tide amplitude
σ = 1.405 19 Z 10^{-4} sec^{-1} = M_2 tide frequency
χ = $2\pi(h_o - s_o)/180$ = M_2 astronomical argument (in rad)
h_o = 279.696 68 + 36 000.768 925 485T + 3.03 Z 10^{-4} T^2
= mean longitude of the sun relative to Greenwich midnight of day D (in deg)
s_o = 270.434 358 + 481 267.883 141 37T − 0.001 133T^2 + 1.9 Z 10^{-6} T^3
= mean longitude of the moon relative to Greenwich midnight of day D (in deg)
T = [27 392.500 528 + 1.000 000 035 6$\bar{D}$]/36 525
$\bar{D}$ = D + 365(Y − 1975) + Int [(Y − 1973)/4]
Int[x] = integral part of x

The corresponding instantaneous ocean partial tide (Schwiderski, 1978a, 1980a) is determined by

$$\zeta = \zeta \cos(\sigma t + \chi - \delta), \tag{2}$$

where the local harmonic constants

$\zeta - \zeta(\lambda, \phi)$ = M_2 ocean tide amplitude (in m)

and

$\delta = \delta(\lambda,\phi)$ = M_2 ocean tide Greenwich phase (in rad)

must be determined, say, by linear interpolation in the tidal charts of Appendix A.

A simple second-order approximation in the sense of Love and Accad and Pekeris (Schwiderski, 1978a, 1980a, c; Accad and Pekeris, 1978) yields

$$\zeta^e \approx 0.612\eta \text{ and } \zeta^{eo} \approx -0.0667\zeta, \quad (3)$$

i.e., the corresponding terrestrial tide ζ^e and the earth dip ζ^{eo} (yielding) under the oceanic tidal load ζ, respectively. A more elaborate and probably slightly more accurate earth dip ζ^{eo} may be computed by using Farrell's Green function (Farrell, 1972, 1973; Pekeris, 1978; Goad, 1980a, b; Schwiderski, 1980a, c). In linear superposition, one finds the corresponding instantaneous geocentric surface M_2 tide:

$$\zeta^s = \zeta + \zeta^e + \zeta^{eo}. \quad (4)$$

A Random-Point Tide (RPTIDE) program is described in Schwiderski and Szeto, 1981a, which computes instantaneous oceanic and/or geocentric partial and/or superposed tides at specified random points from the harmonic constants listed on the NSWC GOTD 1981 Tape (see section "The NSWC Ocean Tide Model"). A much more efficient program to compute instantaneous geocentric tides at large numbers of equidistant points along satellite ground tracks "parallel" to a specified standard satellite track is described in Schwiderski and Szeto, 1981b. A preliminary version of the Satellite-Track Tide (STT) program has been used by the Naval Surface Weapons Center and other institutions to compute instantaneous geocentric tides along SEASAT ground tracks with the leading seven partial tides (M_2, S_2, N_2, K_2) and (K_1, O_1, P_1).

M_2 Ocean Tide Features

The entire constructed M_2 ocean tide is displayed gridwise in map-like amplitude and phase tables in Appendix A. The 42° × 71° charts cover the whole globe north of colatitude 169° (Antarctica) in three zones: a northern zone N from 0° to 71° colatitude, a middle zone M from 48° to 118° colatitude, and a southern zone S from 98° to 168° colatitude. The overlapping geographical areas of the tidal charts have been chosen to provide a worldwide coverage for special applications and to allow the reader to scan the large amplitude and phase charts together in order to evaluate their quality and visualize the important tidal features. In addition, a

generally superficial overview of some tidal features can be recognized by inspecting the plotted corange and cotidal maps provided in Appendix B for the world oceans and the Arctic Sea.

For an easy evaluation of the tidal charts in Appendix A, all hydrodynamically interpolated empirical tidal amplitudes and phases have been marked visibly by subbars for all shore data and by subbrackets for all near-shore deep-sea input constants. Furthermore, the charts display the approximate locations of distant offshore deep-sea stations by subtildes under the computed am-

Table 2
North Atlantic Ocean deep-sea empirical and modeled M_2 Tides.

Long W	*Lat N*	*Emp ξ*	*Mod ξ*	*Δξ*	*Emp δ*	*Mod δ*	*Δδ*	*IAPSO NR*	*Sources*
13°51′	58%16′	83	85	+ 2	168	169	+ 1	1.1.37	C
24°43′	62°50′	90	87	− 3	180	182	+ 2	1.1.29	C
28°46′	60°12′	69	70	+ 1	183	186	+ 3	1.1.30	C
29°58′	57°01′	52	52	0	177	180	+ 3	1.1.31	C
30°10′	53°39′	39	34	− 5	158	158	0	1.1.32	C
25°06′	53°31′	52	48	− 4	145	147	+ 2	1.1.33	C
20°00′	53°39′	69	66	− 3	141	143	+ 2	1.1.34	C
28°11′	48°45′	38	34	− 4	112	111	− 1	1.1.38	C
28°09′	45°21′	41	40	− 1	89	87	− 2	1.1.39	C
27°57′	41°25′	47	47	0	73	73	0	1.1.40	C
20°05′	37°09′	66	66	0	63	64	+ 1	1.1.41	C
14°15′	36°41′	85	83	− 2	68	64	− 4	1.1.42	C
75°38′	32°42′	48	47	− 1	356	357	+ 1	1.2. 3	C, M
76°25′	30°26′	44	45	+ 1	358	2	+ 4	1.2.11	C, P
76°48′	28°27′	41	41	0	2	8	+ 6	1.2.15	C
76°47′	28°01′	40	41	+ 1	9	8	− 1	1.2.14	C
67°32′	28°14′	34	33	− 1	359	3	+ 4	1.2. 5	C, Z
69°45′	28°08′	35	35	0	1	3	+ 2	1.2. 4	C, Z
69°40′	27°59′	34	36	+ 2	359	3	+ 4	1.2. 8	C, Z
69°40′	27°58′	35	36	+ 1	1	3	+ 2	1.2. 7	C, Z
69°20′	26°28′	32	31	− 1	3	5	+ 2	1.2.10	C, Z
69°19′	26°27′	31	31	0	0	5	+ 5	1.2. 9	C, Z

ξ = Amplitudes (cm)
δ = Greenwich Phases (deg)
IAPSO = Int. Assoc. for the Phys. Sci. of the Oceans
C = Cartwright et al. (1979)
M = Mofjeld (1975)
P = Pearson (1975)
Z = Zetler et al. (1975)

plitude and phase data. The corresponding empirical data, which were excluded from hydrodynamical interpolation (Schwiderski, 1978a, 1980b, c), are listed and compared with the modeled data in Tables 2 and 3. Finally, the approximate geographical locations of the important amphidromic points of zero amplitudes are marked by a circled X.

The tidal charts and maps permit the viewer to follow the tidal waves, that is the high water fronts (crests), in forward (or backward) direction, for instance, on their rotation around the amphidromic points. In the tidal phase charts of Appendix A it is best to start from the prominently visible 0° = 360° or 100° cotidal lines. Since the Greenwich phases specify the time lags (in degrees: 30° ≈ 1 hour) of the tidal crests relative to crossing time of the corresponding equilibrium tide along Greenwich meridian (moon's passage over Greenwich meridian; see Schwiderski, 1978a, 1980b, c), one gathers a vivid impression of the significant global and local tidal phenomena.

As was explained by Schwiderski (1978a, 1980b, c), ... follow-

Table 3
Northeast Pacific and southeast Indian Ocean deep-sea empirical and modeled M_2 Tides.

Long	*Lat*	*Emp ξ*	*Mod ξ*	*Δξ*	*Emp δ*	*Mod δ*	*Δδ*	*IAPSO NR*	*Sources*
144°22′W	56°08′N	97	99	+ 2	283	284	+ 1	2.1.17	C
135°38′W	53°19′N	100	102	+ 2	267	265	− 2	2.1.16	C
132°47′W	49°35′N	90	92	+ 2	252	252	0	2.1.15	C
145°00′W	34°00′N	27	26	1	266	270	+ 4	2.1. 9	C, I
145°00′W	34°00′N	27	26	− 1	268	270	+ 2	—	I
124°26′W	27°45′N	29	26	− 3	128	130	+ 2	2.1.13	C, M
129°01′W	24°47′N	19	19	0	107	107	0	2.1.10	C, M
132°01′E	37°01′S	14	14	0	64	64	0	4.1. 1	C, IS
132°09′E	50°02′S	12	12	0	65	68	3	4.1. 2	C, IS
132°07′E	60°01′S	18	17	− 1	79	85	+ 6	4.1. 3	C, IS

ξ = Amplitudes (cm)
δ = Greenwich Phases (deg)
IAPSO = Int. Assoc. for the Phys. Sci. of the Oceans
C = Cartwright et al. (1979)
I = Irish et al. (1971)
IS = Irish and Snodgrass (1972)
M = Munk et. al. (1970)

ing the tidal waves on their periodic rotations, one finds these waves passing through the specially marked stations in empirically correct time and with the correct height. In fact, all over the globe over 2,000 tidal phases and 2,000 amplitudes are coherently integrated. This is particularly impressive for the charts of the Pacific Ocean, where the empirical data from so many clustered and scattered island stations fit smoothly into the surrounding computed tides. From the smoothness features of erratically interpolated tidal data (see "The NSWC Ocean Tide Model"), one concludes that this result is not an artifact of the interpolation applied, but constitutes a vivid manifestation of the excellent compatibility of both the empirical and hydrodynamical procedures combined.

The smooth integration of the empirical tide data into the computed tide model is the basis (Schwiderski, 1978a, b, 1979a, b, c, 1980a, b, c, 1981b, 1983b, d) of the estimated 5-cm tide prediction accuracy that the M_2 model holds over all open ocean areas. This uniform accuracy of the constructed M_2 tide is, of course, fully validated by all 32 empirical tide data from distant offshore deep-sea tide gauge stations that could not be hydrodynamically interpolated into the model (Schwiderski, 1978a, 1980b, c). These excluded data are listed and compared with the corresponding computed data in Tables 2 and 3. The differences (not necessarily errors) range from 0 to 5 cm in amplitudes and 0° to 6° in phases, which is well within the accuracy range of the empirical tide data (see, for instance, final section and Schwiderski, 1978a, 1980b, c, and 1983b).

Naturally, in coastal waters where the empirical tide data are marginal in quantity and/or quality, such as at Arctic and Antarctic shores, a somewhat lesser accuracy must be expected. A similar loss of accuracy must be accepted near rough ocean basin reliefs such as continental shelves and narrow ocean ridges. In these shallow waters, tides are often rapidly varying over short distances and cannot be properly resolved by a 1° × 1° grid system. Fortunately, such rapid tidal variations are well known (see, e.g., Figures 1 and 2) to be confined to small local areas and affect the open ocean tides insignificantly. For special applications of the modeled ocean tides, some simple improvements in coastal

waters as well as in gridwise disconnected border seas are suggested in the final section, in Schwiderski, 1981b, and in Schwiderski and Szeto, 1981a. A further discussion of the M_2 ocean tide model in relation to the other constructed partial tides of the semidiurnal, diurnal, and long-period species may be found in the final synoptic Part XII of this series (Schwiderski, 1983d).

General Applications of the NSWC Ocean Tide Models

Since the publication of the first computed M_2 component (Schwiderski, 1978a), the subsequently constructed eleven-mode NSWC ocean tide models proved their accuracy and usefulness in numerous practical and scientific applications and tests around the world. For example, various empirical tide data from both coastal and deep-sea stations were identified as inaccurately listed and/or harmonically analyzed (see, e.g., "The NSWC Ocean Tide Model," the final section, and Schwiderski, 1979b and 1983b). This result suggests the use of mathematically computed tide models as reference functions to enhance the accuracy of future harmonic analyses of measured tidal time sequences by the widely applied Munk and Cartwright (1966) response method. In a similar self-improving application, NSWC models are used effectively to provide accurate open-ocean boundary data for limited-area tide models where rough water level variations require a refined resolution. For instance, MacAyeal (1982) failed to bring his detailed tide model of the frozen Ross Sea in agreement with empirical tide data, but he succeeded with the help of the global NSWC tide models. This is particularly gratifying, since the NSWC models are admittedly somewhat loosely substantiated near Antarctica, where only quantitatively and qualitatively marginal empirical tide data are available.

In marine geodesy, NSWC tide models are used extensively (see, e.g., Resolutions of the NASA SEASAT ALT/POD Calibration Workshop, June 11–15, 1979, Austin, Texas; West, 1981) to compute tide corrections for satellite altimeter measurements of the geoid at sea. In geophysics, the same tide models were used successfully by Wahr and Sasao (1981a,b) to verify their theoretically

predicted resonant coupling between the nutations of the earth spin axis and the terrestrial and oceanic tides. Similarly, Sasao and Sato (1981) computed meaningful ocean tide corrections for astronomical time and latitude observations. Utilizing NSWC models, preliminary investigations by Van Ruymbeke et al. (1981) and others did suggest that the turning ocean tide may provide a clock and a clue for a better understanding of the triggering mechanism of earthquakes.

After successful applications to worldwide measurements of gravity anomalies down to about 1/2 microgal (see, e.g., Goad 1980a, b; Melchior et al. 1980, 1981), the NSWC ocean tide models were chosen by the International Permanent Commission for Earth Tides (see Resolutions of the Ninth Earth Tide Symposium, August 17–22, 1981, New York, N.Y.) as a "Working Standard" for the interpretation of earth tide data, for predictions of earth tidal displacements and gravity anomalies, and for tidal loading calculations. This resolution was accepted by all participants, even though a considerable number of empirical gravity anomalies could not be verified by the NSWC ocean tide models. While it was pointed out by the author (Schwiderski, 1981b) that some of the differences could probably be explained by shortcomings and simple improvements (see final section) of the ocean tide models, particularly in coastal areas, it was generally recognized that the major discrepancies must be attributed to oversimplifications of the solid earth body and the corresponding earth tide and ocean tide loading models. Among the many researchers who expressed the same view about these or related problems, perhaps the most prominent statement by Farrell (1979; compare also Farrell et al., 1982) may be quoted here: "The cause of these anomalies is now known to be inhomogeneities in the elastic properties of the earth crust . . . variable surface topography and geological discontinuities . . ." In fact, far beyond such geophysically plausible reasons, recently Melchior and DeBecker (1982) proved that all significant differences between gravity anomalies measured around the world by various investigators and those computed from earth tide models, NSWC ocean tide models, and their loading effects are exclusively due to the earth tide models used. Since these models are all based on horizontally homogeneous deformation

parameters of the solid earth, the sources of the discrepancies are obvious (see also final section), and they are found to be most severe in seismically and/or tectonically active areas of the earth. It is hoped that future accurate gauge measurements of ocean tides and satellite altimeter measurements of geocentric tides will lead to useful and long needed laterally variable deformation parameters of the solid earth.

Spherical Harmonic Coefficients of M_2 Ocean Tides

The secular tidal deceleration of the lunar longitude and its importance in astronomy has been recognized by scientists for almost three centuries. However, as reviewed for instance by Cartwright (1977), the empirical and theoretical estimates diverged by more than a factor of 10. With recently improved observations and better knowledge of ocean tides, the estimates finally seem to converge within the accuracy limitations of the contemporary measurements, postulated earth and ocean models, and numerical computations involved in the estimation process. Since this certainly somewhat subjective viewpoint is not shared by all researchers in the field (compare, e.g., Marsh et al., 1982; Yoder, 1982), the following brief examination of the basic concepts and results may help in clarifying the present situation.

If one assumes a solid earth body and corresponding earth tide and ocean tide loading models, then it is possible (Lambeck et al., 1974) to compute the secular deceleration effects of the moving ocean tidal masses on the orbits of the moon and artificial satellites from an assumed ocean tide model. Vice versa, it is in principle possible to derive from observed decelerations of satellite orbits certain global earth and/or ocean tide parameters. This possibility is attractive, even though neglected lateral variations of the solid earth were found (see preceding section) to have a measurable effect on nearby gravity meters. In distinct contrast to the related problem of near-earth gravity anomalies, globally integrated lateral variations of the solid earth probably can be neglected as essentially ineffective on distant satellites. Though the same arguments should apply also to minor and/or localized in-

accuracies of ocean tide models, some researchers feel tempted (see, e.g., Yoder, 1982) to blame any differences between empirical and theoretical results on assumed ocean tide models. In reality, however, both the empirical and theoretical results are limited by inherent error sources, which have nothing to do with the accuracy of the assumed ocean tide model.

The mathematical linkage between the ocean tide and its deceleration effect on an orbiting satellite begins with a Fourier spherical harmonic expansion of a given harmonic partial ocean tide ζ (say, M_2; for notations see "Parameters of M_2 Ocean Tide Model") in the form

$$\zeta = \zeta(\lambda, \phi, t) = \sum_{n=o}^{\infty} \sum_{m=o}^{n} P^m_n(\sin\phi) \left[C^{\pm}_{mn} \sin(\sigma t + \chi + \epsilon^{\pm}_{mn} \pm m\lambda) \right] \quad (5)$$

where $P^m_n(x)$ denotes the associated Legendre polynomials in standard norm ($P^o_n(1) = P_n(1) = 1$). The constant (in time and space) harmonic amplitudes $C^{\pm}_{mn}$ and phases $\epsilon^{\pm}_{mn}$ must be determined in the Fourier sense by a least-squares fit to the tidal data ζ over the entire globe with $\zeta \equiv o$ on land. For the present M_2 ocean tide model C. C. Goad (private communication) computed numerically these constants up to degree $n = 10$. The most important coefficients are listed in Table 4. The author verified those results and recomputed these coefficients with a slightly improved tide model by shifting (see final section and Schwiderski, 1981b) all hydrodynamically interpolated empirical coastal tide data from the

Table 4
Important spherical harmonic fourier constants of M_2.

Constant	C^+_{oo} (cm)	C^+_{22} (cm)	C^+_{24} (cm)	ϵ^+_{oo} (deg)	ϵ^+_{22} (deg)	ϵ^+_{24} (deg)
Goad	.25	2.96	1.01	118.1	310.6	124.8
Author[a]	.16	2.95	1.00	106.2	311.6	125.2

[a] Improved values (see text)

tabulated cell centers to the more accurate corresponding land cell walls. As can be seen in Table 4 only C^{+}_{∞} and ϵ^{+}_{∞} display a significant improvement. The corrected data locations were expected to improve these results, because $C^{+}_{\infty}(=C^{-}_{\infty})$ measures one half of the small periodic inflow (or outflow) of water over the mathematically defined ocean boundaries, which is allowed by the hydrodynamical interpolation technique (see Schwiderski, 1980b,c). Incidentally, this result provides important evidence for the high precision with which the continuity equation has been solved in the interior of the oceans.

Regardless of the quality of the assumed ocean tide data ζ, the serious deficiencies of any truncated expansion (5) has been discussed extensively in Schwiderski, 1980c. It suffices to recall here the following critical features relevant to the application considered. Due to the strong discontinuities of the expanded function $\zeta(\lambda,\phi,t)$ along all land–ocean interfaces, the series (5) is very slowly converging, and any truncated sum is afflicted with the well-known Gibbs phenomenon. For the present M_2 tide model Goad (1980b) computed the amplitude spectrum up to 180° and confirmed the unacceptably slow convergence. Since the Fourier representation (5) of the expanded ocean tide ζ is unsatisfactory for any computationally useful truncation, Estes (1980) abandoned the Fourier expansions for his tide models and replaced them by non-Fourier type trignometric polynomial fits to ζ by least-squares over the oceans only and ignored all land areas. Though this yields significantly better fits to the ocean tides, it is obviously not applicable to the present problem of satellite decelerations.

Still more important is the fact that the intensity of the Gibbs phenomenon increases with the length of the partial sum and in the numerical case also with the number of grid points used. Consequently, the accuracy of all numerically computed constants (C,ϵ) in the Fourier expansion (5) depends in some measure on the grid system on which the tide data ζ are defined. Unfortunately, this holds true also for the low degree constants such as C^{+}_{22}, which plays the most important role in the deceleration problem at hand. To assess the accuracy dependence of the Fourier coefficients on the number of grid points, Goad and Douglas (1978) computed from the author's preliminary M_2 ocean tide model (1975, unpub-

lished) C^{+}_{22} for various mesh sizes, as shown in Table 5. Accordingly, varying the mesh size from 1° to 10° results in an erratic change of C^{+}_{22} by more than 0.5cm, which has nothing to do with the quality of the tide model considered.

To derive empirically the low-degree Fourier coefficients of the M_2 ocean tide (5) from observed satellite decelerations, the earth tide effect must be subtracted. This requires accurate knowledge of the solid earth tide, especially in relation to its tide-generating equilibrium tide. As was justified above, all investigators assume a horizontally homogeneous earth and, furthermore, perfectly elastic body properties. The latter assumption leads to earth tides that are exactly in phase with the tide-generating equilibrium tides. Although the ideal earth assumption is probably very close to reality, it is definitely not exactly true. To estimate the effect of an assumed small earth tide phase lag on the low-degree Fourier coefficients of the ocean tide ζ, Goad and Douglas (1978) computed Table 6 for C^{+}_{22} from GEOS 3 and combined GEOS 3/1967-92A orbits. As can be seen, a small earth tide phase lag of just one half degree reduces C^{+}_{22} by almost 0.5 cm and by almost 1 cm for a one-degree phase lag.

Table 5
Mesh size dependence of C^{+}_{22} for preliminary NSWC M_2 Model (1975).
(Computed by Goad and Douglas, 1978)

Mesh Size	*1°*	*3°*	*5°*	*8°*	*10°*
C^{+}_{22} (cm)	3.59	3.65	3.38	3.81	3.26

Table 6
Dependence of C^{+}_{22} on earth tide phase lags.
(Computed by Goad and Douglas, 1978, from
GEOS 3 and Combined GEOS 3/1967-92A orbits)

Assumed Phase Lag	*0.0°*	*0.5°*	*1.0°*
GEOS 3 orbit: C^{+}_{22} (cm)	2.86	2.39	1.95
GEOS 3/1967-92A: C^{+}_{22} (cm)	3.23	2.76	2.32

Another major uncertainty in the empirical determination of, say, C^+_{22} for M_2 follows from the always controversial harmonic analysis of time sequences with a nonharmonic frequency spectrum. Moreover, this error source afflicts the earth and ocean tides and their gravitational consequences. In particular, the beat effect of the M_2 group elaborated in the final section generates alone an amplitude uncertainty of 4.8% in both ocean and earth M_2 tides. Assuming an oceanic C^+_{22} of about 3 cm (Table 4), one has a source for an error of 0.15 cm. Since the M_2 earth tide has an amplitude of about $E \approx 15$ cm (see Equation 3), the beat effect translates into a possible empirical error of 0.71 cm (see Table 7).

Considering only the three elaborated processing uncertainties (each of 0.5 cm and more) in a direct ocean tide solution (Table 5) and in an indirect satellite solution (Tables 6 and 7), the recently published results displayed for M_2 in Table 8 must be viewed as closely (almost fortuitously) converged as could be wished for. In fact, it is rather gratifying to find the author's value of 2.95 cm safely below the satellite average of 3.11 cm. The remaining small margin allows for a small but definitely nonzero earth tide phase lag (see Table 6). The same continues to be true, even if one ignores the two lowest satellite solutions to yield the average 3.26 cm.

The table of ocean tide solutions (Table 8) fully confirms the earlier argument that relatively small or locally confined errors of ocean tide models are averaged out globally in C^+_{22} and, hence, are just as ineffective on distant satellites as neglected lateral variations of earth tide models. For example, the results in Table 4 show that the significant relocation of empirical tide data in about 2,000 boundary cells may effect drastically some weighted averages $(C^+_{00}, \epsilon^+_{00})$ and leave others $(C^+_{22}, \epsilon^+_{22})$ almost unchanged.

Table 7
Beat effects in M_2 group on earth and ocean tides.

M_2 Tidal Amplitude	*Beat Effect*
Earth tide: $E = 15$ cm	0.71 cm
Ocean tide: $C^+_{22} = 3$ cm	0.15 cm

Table 8
Recent results of M_2 ocean tide coefficients C_{22}^{+}.

$C_{22}^{+(cm)}$	*Model Characteristics*
	Ocean Tide Solutions
3.59	1° Schwiderski (1975; unpublished)
3.31	3° Estes (1977, 1980)
2.95	1° Schwiderski (1978a)
3.38	6° Parke and Hendershott (1980)
	Satellite Solution
3.10	Cazenave and Daillet (1977; Starlette)
3.20	Daillet (1978; GEOS 3/Starlette)
2.86	Goad and Douglas (1978; GEOS 3)
3.23	Goad and Douglas (1978; GEOS 3/1967-92A)
3.42	Felsentreger et al. (1979, GEOS 3/1967-92A/Starlette)
3.50	Cazenave and Daillet (1981; Starlette)
3.10	Cazenave and Daillet (1981; GEOS 3/Starlette)
2.50	Marsh et al. (1982; Starlette)
3.11	Average satellite solution

Moreover, the differences in the ocean solutions exhibit precisely the same spread as the grid-generated erratic variations in Table 5. In this connection it is important to recall the major features of the four ocean tide models compared in Table 8. The Estes (1977) and the author's (1975, preliminary unpublished) ocean tide models are both hydrodynamical solutions of very similar ocean tidal equations derived from the Navier-Stokes equations with turbulent bottom friction and eddy dissipation terms. Both solutions displayed similar significant improvements over earlier models, but still failed to match empirical tide data over considerable ocean regions. The author's (1978) model is still a complete hydrodynamical solution (for evidence see above and next section) of the same ocean tidal equations, but with more realistic eddy dissipation and empirically adjusted bottom friction terms. The agreement with empirical tide data around and in the oceans is exhaustively complete (see first section) within the empirical accuracy. Without regard to any hydrodynamical equations the Parke-Hendershott model is strictly a least-squares fit of a linear superposition of some 24 numerically defined base functions to

selected empirical tide data in the oceans (see Parke and Hendershott, 1980: 383, 384, 388). Attempts to compute the corresponding velocity field via the Laplace tidal equations (which are derived from the drastically simpler Euler–Lagrange equations) appeared to run into "unresolved numerical problems" in kinetic energy calculations (see also next section). Of course, the graphically displayed tide model is close to the author's (1978) model over most open ocean regions, since both models fit essentially the same empirical open-ocean tide data. Consequently, even though both models differ considerably in coastal and some other areas, where the 6° × 6° model naturally fails to resolve virtually all tidal distortions (such as shown in Figures 1 and 2), one should expect their corresponding C^{+}_{22} coefficients to be close together. Yet, as Table 8 shows, the Parke–Hendershott (see also next section) C^{+}_{22} is considerably closer to the author's (1975) preliminary value. Clearly, the magnitude of the global C^{+}_{22} coefficients does not reflect the point-wise closeness of the corresponding tide models. This shows once again that the C^{+}_{22} coefficient is no measure for the quality of an ocean tide model. In any case, it cannot override an accuracy estimate concluded from a model's fit to thousands of empirical tide data derived from ocean tide gauge records around the world.

The Energy Budget of Ocean Tides

In order to understand the historical evolution of the solar system and the physical properties of the earth and oceans, scientists have long been interested in the fate of the energy that is continuously supplied to the oceans by the tide-generating forces of the moon and sun. Clearly, through the relentless turbulent oscillations of the water masses, the supplied tidal energy is constantly lost by eddy dissipation into heat and other internal ocean energy, and by friction and displacement interactions with the solid earth into mechanical earth energy. But, is all the supplied tidal energy dissipated that way, and in what proportions? Early answers to these questions depended on insufficiently accurate ocean tide models, which led to widely diverging estimates and conflicting discrepancies (see, e.g., Cartwright, 1977). Surely, reliable answers to

these questions require accurate knowledge not only of the tidal elevations but also of the much more involved velocity fields and turbulent dissipation and friction parameters. Since the present M_2 ocean tide model can be assumed to provide all these necessary data with realistic accuracy, the following detailed analysis can be anticipated to shed some light into the situation.

Starting from the continuous ocean tidal equations derived from Schwiderski (1978a, 1980a, c), it is easy to derive the corresponding energy equation in the following form:

$$\rho GHq\cdot\nabla\hat{n} = [-\rho G\zeta_t^b(\zeta+H)]+\rho bq^2\cos\phi+\rho q\cdot f+\rho G[\zeta^b(\zeta+H)+\tfrac{1}{2}\zeta^2]_t +\tfrac{1}{2}\rho H(q^2)_t+\rho G\nabla\cdot(qH\zeta^s) \tag{6}$$

or averaged over one harmonic time period and integrated over the closed oceans:

$$\text{RSTE} = \text{RBDW} + \text{RBFW} + \text{ROED} = \text{RLTE}, \tag{7a}$$

where

$$\text{RSTE} = \begin{cases} \rho G\iint_{\text{c.o.}} <\zeta_t\hat{n}>\,da \\ \text{Rate of Supplied Tidal Energy} \end{cases}$$

$$\text{RBDW} = \begin{cases} \rho G\iint_{\text{c.o.}} <\zeta_t\zeta^b>da = -\rho G\iint_{\text{c.o.}} <\zeta\zeta_t^b>da \\ \text{Rate of Bottom Displacement Work} \end{cases} \tag{7b}$$

$$\text{RBFW} = \begin{cases} \rho b\iint_{\text{c.o.}} <q^2\cos\phi>da = \text{RSBFW} + \text{RDBFW} \\ \text{Rate of Bottom Friction Work,} \end{cases}$$

$$\text{RSBFW} = \begin{cases} \rho b\iint_{\text{a.o.}} <q^2\cos\phi>da \\ \text{Rate of Shelf Bottom Friction Work} \end{cases} \tag{7c'}$$

$$\text{RDBFW} = \begin{cases} \text{RBFW} - \text{RSBFW} \\ \text{Rate of Deep Bottom Friction Work} \end{cases} \tag{7c''}$$

$$\text{ROED} = \begin{cases} \rho \iint_{\text{c.o.}} \langle q \cdot f \rangle da = \text{RSTE} - \text{RBDW} - \text{RBFW} \\ \text{Rate of Ocean Eddy Dissipation} \end{cases} \tag{7d}$$

$$\text{PFCL} = \begin{cases} \rho G \iint_{\text{c.o.}} \langle \nabla \cdot qH(\hat{\eta} - \zeta^B) \rangle da = \rho G \int_{\text{c.l.}} \langle q_n(\hat{\eta} - \zeta^B) \rangle ds = o \\ \text{Power Flux Over Coastline} \end{cases} \tag{7e}$$

$$\text{RLTE} = \begin{cases} \text{RBDW} + \text{RBFW} + \text{ROED} \\ \text{Rate of Lost Tidal Energy} \end{cases} \tag{7f}$$

and furthermore:

$$\text{KE} = \begin{cases} \frac{1}{2}\rho \iint_{\text{c.o.}} \langle Hq^2 \rangle da \\ \text{Kinetic Energy} \end{cases} \tag{8a}$$

$$\text{PE} = \begin{cases} \rho G \iint_{\text{c.o.}} \langle \zeta^b(\zeta + H) + \frac{1}{2}\zeta^2 \rangle da \\ \text{Potential Energy} \end{cases} \tag{8b}$$

$$\text{TE} = \begin{cases} \text{KE} + \text{PE} \\ \text{Tidal Energy} \end{cases} \tag{8c}$$

In these equations the following notations are used in addition to those already introduced in "Parameters of M_2 Ocean Tide Model" (compare also Schwiderski, 1978a, 1980a,c):

b	=	bottom friction coefficient
H	=	ocean depth
R	=	earth radius
ρ	=	density of seawater
ζ^b	=	$\zeta^e + \zeta^{eo}$ = geocentric bottom tide
$\hat{\eta}$	=	$1.302\eta + 0.0333\zeta$ = total tide-generating equilibrium tide
q	=	(u,v) = velocity vector corresponding to (λ,ϕ)
q_n	=	velocity normal to coastline
f	=	(f^λ, f^ϕ) = eddy dissipation vector
$\triangle$	=	$1/R(1/\cos\phi\partial\lambda, \partial\Phi)$ = differential vector
$\langle x \rangle$	=	average over tidal period
da	=	ocean surface element

ds = ocean boundary element
c.o. = closed ocean
s.o. = shelf ocean
c.*l*. = coastline

Using the present M_2 ocean tide model with all its resolved parameters and tide data (ζ;u,v), the global quantities (7a,b,c,d) and (8a,b,c) were evaluated numerically with the detailed results shown in Table 9. This table lists also three different Q factors of ocean tides, which appear useful by their self-explanatory definitions.

Naturally, the numerically computed global ocean tide data in Table 9 must be viewed as representative values within certain error bounds. Fortunately, as in the similar global computations of Fourier coefficients (see preceding section) minor inaccuracies of the modeled tide data can be assumed as averaged out. On the

Table 9
M_2 ocean tide energy budget.

Rate of Supplied (+) and Lost (−) Energies			
(+) RSTE (10^{12} Watt)	3.50		
		1.86	
(−) RBDW (10^{12} Watt)	1.64		
		3.50	
(−) RBFW (10^{12} Watt)	1.86		3.50 = RLTE (−)
		1.86	
(−) ROED (10^{12} Watt)	0.00		
(−) RSBFW (10^{12} Watt)	1.26		
		1.86 = RBFW (−)	
(−) RDBFW (10^{12} Watt)	0.60		
Stored Ocean Tide Energies			
PE (10^{17} Joule)	1.07		
		2.53 = TE(10^{17} Joule)	
KE (10^{17} Joule)	1.46		
Q Factors of Ocean TIdes			
σ (TE) / (RLTE)	10.2 = Q (lost work)		
σ (TE) /RBFW	19.1 = Q (bottom friction)		
σ (TE) /RSBFW)	28.2 = Q (shelf bottom friction)		

other hand, some dependence on the grid size must again (see Table 5 and below) be admitted to effect the accuracy of the energy data. Since the present computations required the tidal velocities in addition to the well-verified tidal elevations, several numerical experiments were conducted to test the periodic state of the velocity data reached by the time-stepping integration of the discrete ocean tidal equations (see Schwiderski, 1978a, 1980a,b,c). These checks were considered necessary, because it is much more difficult to compute the velocity field than the less variable tidal (pressure) field. For these experiments the computations of the M_2 integration were continued from the last final output through 1/4, 1/2, and 1 full M_2 periods. The recomputed steady state velocity amplitudes and phases displayed changes of less than 10% over all open ocean areas. Somewhat larger variations were expected and found near coastal boundaries. As anticipated from these satisfactory results, the recomputed global energy data in Table 9 remained essentially unchanged. The fact that Equations (7 and 7d) are fulfilled within the numerical accuracy of three figures and ROED $\approx 0.00 \times 10^{12}$ Watt (Table 9) is an important manifestation of the precision of the computed tidal elevation and velocity fields as a solution of the ocean tidal equations with determined bottom friction and eddy dissipation coefficients.

A glance at Table 9 reveals the surprising result that the rate of supplied tidal energy (RSTE) equals the rate of lost tidal energy (RLTE) without any significant gaps, which have puzzled researchers (see, e.g., Cartwright's 1977 review) since Hendershott (1972) lumped RSTE and RBDW together as "total rate of work done on the oceans." It was tacitly assumed that the rate of bottom displacement work (RBDW) would be positive, i.e., the ocean bottom would do positive work on the ocean and, hence, add to the energy input RSTE by the tide-generating gravity forces. However, as was pointed out by the author at the NASA Workshop on Ocean Tides from April 12 to 13, 1982, at the University of Chicago, Illinois, the separate computation of RBDW turned out a negative value. As is evident from Equation (7b), the ocean tide does work on the earth and not the other way around. Obviously, this closes the puzzling major gap of the missing energy sink and corrects most interpretations of previous estimates.

The subsequent detailed evaluation of the energy budget must recognize two additional error sources that may influence somewhat the magnitudes of some individual energy terms. Firstly, the energy equation (7) is based on the plausible assumption that the power flux over the coastline of a closed ocean is zero (PFCL $\approx$ 0, Equation 7e). Unfortunately, the real ocean basins have no well-defined boundary walls or coastlines. The gridwise modeled ocean boundaries follow only approximately the already ambiguous coastline and exclude various shallow regions with less than 5-m depth and border seas (see Schwiderski, 1978a, 1980a,b,c). Thus, Equation (7e) and similarly the right part of Equation (7a) must be considered as approximations. Their precise errors can be assessed only by means of future refined coastal tide models. Nevertheless, considering estimates in border seas (see, e.g., Miller, 1966, and Cartwright et al., 1980) the computed value of RSTE = 3.50Z10^{12} Watt is probably a close low estimate of the true value. It agrees perfectly with Cartwright's (1977) estimate of $3.5 \cdot 10^{12}$ Watt, which he concluded from various theoretical and empirical evaluations. Obviously, the present result cannot be compared with the drastically reduced value of $2.22 \cdot 10^{12}$ Watt, which Parke and Hendershott (1980: 388) computed as the "rate of lunar working." It represents the lumped value (RSTE-RBDW) and must be compared to the corresponding value of $1.86 \cdot 10^{12}$ Watt listed in Table 9. The agreement appears satisfactory within the possible numerical error resulting from the mesh size differences of both models (see Table 5 and preceding section).

The other possible error source is a direct consequence of the linear bottom friction law and the numerical value of its coefficient b, which is used in the definition of the rate of bottom friction work (RBFW, Equation 7c, and also c′, c′′). Although it was recognized that in some shelf areas with strong tidal currents the quadratic law of bottom friction would probably be slightly more appropriate, it was argued (see below and Schwiderski, 1978a, 1980a,b,c) on hydrodynamical grounds that the linear law of bottom friction should be the most consistent and realistic hypothesis at least for slow tidal currents as in all deep oceans. For M_2 the value of the bottom friction coefficient b (= 0.01m/sec) was determined by extensive trial-and-error experiments to fit em-

pirical tide data as closely and uniformly as possible over all ocean regions. To fit as closely as possible empirical tide data in boundary cells, the novel hydrodynamical interpolation technique allowed the uniform value of b to vary between the controlled limits 0.003 m/sec $< b \leq$ 0.03 m/sec. An inspection of these variations seemed to indicate that the higher deviations slightly dominated the lower ones. Consequently, the computed value of RBFW = $1.86 \cdot 10^{12}$ Watt (and particularly its shelf contribution RSBFW, see below) is probably a close low estimate of its true value. In any case, it could only exceed this estimate by as much as RSTE may exceed its estimate (see above). Incidentally, the determination of the numerical value of b may be compared to G. I. Taylor's (1918; and Proudman, 1952) fixing of the famous coefficient 0.0026 in the quadratic law of bottom friction. In the present case, b is determined to fit empirical tide data simultaneously with the integration of the global ocean tidal equations. The resulting balanced energy budget (see above) is then only a test for the quality of the integration. Taylor assumed rough empirical tide and velocity data for the Irish Sea and fixed the corresponding friction coefficient to achieve a balanced energy budget. In order to compare the computed rate of bottom friction work (RBFW) with other semiempirical estimates of tidal energy losses over continental shelves, it was necessary (and hydrodynamically important) to compute also the rate of shelf bottom friction work (RSBFW) and, simultaneously, the rate of deep bottom friction work (RDBFW) by Equations (7c′,c′′). In this computation the shelf regions were defined by depth data less than 1,000 m. The corresponding area was about 8% of the entire modeled ocean surface, which is 69% of the global earth area. However, the resulting value of RSBFW = $1.26 \cdot 10^{12}$ Watt cannot be compared directly with Miller's (1966) currently most reliable (see, e.g., Cartwright, 1977) semiempirical estimate of (1.4 to 1.7)$\cdot 10^{12}$ Watt for the total power flux from the deep oceans over the shelf edges to the shelf regions. Since this energy essentially is lost over the shelves by bottom friction and bottom displacement work, an appropriate proportion of the latter must be added to RSBFW for just comparison. Taking a simple shelf/deep-ocean area proportion of 8/92 from RBDW = $1.64 \cdot 10^{12}$ Watt modified by an approximate shelf/deep-ocean tidal

elevation ratio of 2/1 and adding it to RSBFW, one finds $1.50 \cdot 10^{12}$ Watt, which falls well between Miller's estimated limits and is actually closer to his preferred lower bound.

Cartwright et al. (1980) arrived at a semiempirical estimate of energy losses around the British Isles, which is somewhat larger than Miller's corresponding partial value, but they acknowledge that this may easily be compensated by Miller's excessive estimate of the energy loss over the Bering Sea shelf. Furthermore, as is pointed out by the same authors, the semiempirical methods lead to significantly unbalanced energy budgets. Since the contradictory budget terms cannot be accounted for by relatively small energy losses through bottom displacement work (see above), their origin must be sought in the semiempirical methods themselves. Starting from computed gradients of empirical tidal elevations, needed velocities are computed by locally solving Laplace's momentum equations of tidal motions, which are augmented by G. I. Taylor's quadratic bottom friction term that may be linearized under the transplanted conditions (see, e.g., Cartwright et al., 1980: 104, 106, 109). Subsequently, the resulting velocities are used to compute the rate of bottom friction work with G. I. Taylor's friction term and the corresponding power flux, which usually turns out significantly larger than the friction work. Since G. I. Taylor's friction term was derived by balancing the tidal energy budget in the Irish Sea (see above), it is by no means trivial that it should apply universally, say, to all shelf regions from the deep oceans to the shores. The contradictory results are compelling evidence to the contrary. In fact, Proudman (1952: 316) quotes investigations of tides in the Bristol and English channels with variations of G. I. Taylor's constant of 0.0026 down to 0.0014 and up to 0.0213. Clearly, variations of this magnitude can change estimates of power fluxes and rates of bottom friction work considerably. It would be most interesting to see which friction constants in the quadratic and linear bottom friction laws would balance the energy budget around the British Isles. If the quadratic friction law is applied to the global shelf regions and there properly linearized (Proudman, 1952: 310) with an average shelf velocity of 0.1 m/sec and a $\cos \phi$ average of 0.795, then the present value of $b = 0.01$ m/sec requires a 36 times larger G. I. Taylor

constant, i.e., 0.094. However, if the quadratic law is linearized under Irish Sea conditions with an average velocity of 1.14 m/sec and the same cos ϕ average, then the present b = 0.01 m/sec requires a G. I. Taylor constant of 0.0082, which is very well within the known variation range.

As can be verified in Table 9, of the total energy loss by bottom friction about two thirds are lost over the shelf areas and only one third over the deep oceans. Though the latter portion is, as expected, significantly smaller than the first one, it does not justify its neglect in the energy budget as is commonly assumed in semiempirical estimates based on G. I. Taylor's low quadratic friction term (see above and below). In view of the more realistic linear law of bottom friction, this result appears as plausible, because 92% of the ocean bottom is deeper than 1,000 m. One derives from the quadratic equations of bottom friction work (Equations 7c, c', c''), the work ratio (RSBFW)/RDBFW) = 1/2 and the shelf/deep-ocean area ratio 8/92, that the average shelf velocity is about five times larger than the average velocity in the deep oceans. Again, this ratio appears as realistic and is, of course, in agreement with the computed velocity field. Moreover, since the linear law of bottom friction yielded realistic results in its somewhat uncertain shelf domain, the result in the deep ocean should be even more credible. Because the numerical value of the bottom friction coefficient b was allowed to vary in shelf grid cells by the hydrodynamical interpolation technique (Schwiderski, 1978a, 1980a,b,c), its uniform value was determined essentially by the deep oceans in a rather sensitive manner. In fact, numerous experiments were conducted to suppress bottom friction in the deep oceans by assuming, for instance, b ~ 1/H, but they all resulted (with and without hydrodynamical interpolation of empirical tide data) in significant reductions of the model's quality.

In order to understand the physical presence of the underestimated rate of bottom friction work in the deep and shelf oceans, it is necessary to retrace the detailed hydrodynamical derivation of the continuous and discrete ocean tidal equations (Schwiderski, 1978a, 1980a,b,c). Here, it suffices to recall the relevant major concepts and notions that were introduced and extensively analyzed. It was shown that the viscous tidal motion is highly unst-

able, turbulent, and, hence, nonperiodic, and unlike laminar flows microscopically unpredictable. For the macroscopical description of the tidal motions, average velocities were introduced that were strictly tied to mass fluxes through finite mesh areas during finite time intervals. These velocities were assumed to behave just like ordinary (point or particle) velocities of laminar motions with steady-state amplitudes, frequencies, and phases locked to the periodic tidal forcing. In the deep oceans the corresponding average tidal currents are known to be slow and, hence, justify Stokes slow-motion linearization of the equations of motion, including (consistently) a linear bottom friction law.

Following Reynolds the differences between the average velocities and the true tidal (particle) velocities were introduced as velocity fluctuations. Though they are filtered out in the average velocities, they make their presence felt through additional Reynolds stresses that the tide-generating forces must overcome. The Boussinesq approximation treats those stresses like laminar viscous stresses, but with a replacement of the molecular viscosity by two (horizontal and vertical) momentum austausch coefficients or eddy viscosities. While the horizontal coefficient enters directly in the lateral dissipation vector f of Equation (6), the vertical eddy coefficient determines essentially the magnitude of the bottom friction coefficient b. Consequently, the unpredictable fluctuating currents manifest themselves as undetermined eddy viscosities and bottom friction coefficients. Unlike the molecular viscosities, they are not uniform properties of given fluids but characteristic quantities of the specific turbulent flows and their assumed divisions into averaged and fluctuating currents. Although they may be guessed a priori, in general they must be modeled by trial-and-error experiments simultaneously with the entire average tidal elevation and velocity fields to achieve a posteriori verifiable realistic features. Obviously, this is the basic technique applied in the present global tide model and in G. I. Taylor's empirical balancing of the tidal energy budget in the Irish Sea.

As was shown before, G. I. Taylor's quadratic friction term allowed no direct transplantation from the Irish Sea to the global shelf regions without serious numerical shortcomings. With a typical shelf/deep-ocean velocity ratio of 5/1, the discrepancies are

five times compounded if the quadratic friction law is directly applied to the deep oceans. Specifically, a 180 times larger G. I. Taylor constant of 0.47 is required to achieve the same realistic results as the present linear friction coefficient b = 0.01 m/sec. At this point it is interesting to note that the ratio of the required G. I. Taylor deep-ocean/Irish-Sea constants is representable in the form:

$$0.47/0.0026 \approx 180 \approx 0.795(111)^2/(9.56)^2 \cos 53.3°$$

where $0.795Z(111\ \text{km})^2$ is the average bottom mesh area of the present 1° × 1° global ocean tide model. Accordingly, $(9.56\text{km})^2 \cos 53.5°$ can be interpreted as a proper resolution area of the Irish Sea. This interesting relationship supports the author's hypothesis that eddy viscosities and their related bottom friction coefficients should depend directly on the assumed area resolution scales. As was mentioned in Schwiderski (1978a, 1980a,b,c), some dependence of these hydrodynamical parameters on resolution scales was noticed earlier by researchers modeling general ocean currents and atmospheric circulations.

In contrast to the quadratic bottom friction law, the linear law can be transplanted directly, say, from the Irish Sea to the global oceans without encountering major numerical problems. Surely, the tidal budget in the Irish Sea could have been balanced just as well with the linear law of bottom friction. A simple recalculation of G. I. Taylor's balancing procedure yields then a linear friction coefficient of b = 0.0032 m/sec, which is easy to reconcile with the present global (shelf and deep ocean) value of b = 0.01 m/sec. For instance, the variations of G. I. Taylor's constant for the Bristol and English channels (see above) can account directly for the modest 3.1 difference factor. Indeed, the remaining difference may yield an important key to separate the energy losses by bottom friction of the averaged tidal currents from those of the fluctuating currents, both of which must be supplied by the tide-generating forces. It is the author's contention (Schwiderski, 1978a, 1980a,b,c) that the coarse 1° × 1° resolution scale of the global oceans leaves many more fluctuating current modes unresolved than the finer (see above) scale of the Irish Sea. It is probably

reasonable to assume that the contribution of the fluctuating currents to the bottom friction work is negligible in the Irish Sea. If one assumes further that the linear bottom friction coefficient computed above for the Irish Sea is directly transferable to the bottom friction work of the averaged tidal currents in the deep oceans, then one has a procedure to estimate its magnitude. Using Equations (7c,c',c'') with $b = 0.0032$ m/sec instead of 0.01 m/sec, which yielded RDBFW = 0.60 Watt (Table 9), then one finds $0.19 \cdot 10^{12}$ Watt as a possible high and, trivially, $0.00 \cdot 10^{12}$ Watt as a low estimate of the rate of deep bottom friction work done by the averaged tidal currents. The remainders of the total RDBFW yield, respectively, $0.41 \cdot 10^{12}$ Watt and $0.60 \cdot 10^{12}$ Watt as low and high estimates for the rate of deep bottom friction work done by the fluctuating tidal currents. Even though the heuristically inferred nontrivial estimates must be considered as somewhat tentative, it will be shown below that they fit presently known estimates remarkably well.

To establish a proper basis for comparison of the present estimates with other known results, it is necessary to identify the classical hydrodynamical notions of averaged and fluctuating tidal currents with their essentially equivalent concepts of surface (or barotropic) and internal (or baroclinic) tidal currents, respectively. Clearly, the deterministic and random features (Cartwright, 1977; Munk et al., 1981) of surface and internal tidal currents are directly comparable with the predictable and unpredictable properties of averaged and fluctuating tidal currents inferred above from the strong instability of tidal motions. Strong internal currents with amplitudes exceeding considerably the amplitudes of surface currents have been discovered in the deep oceans for some time. Theoretically, they have been analyzed by spectral decompositions starting with wave lengths of 200 km or 150 km (Wunsch, 1975; Munk et al., 1981), which are just about at the resolution limit (111 km) of the averaged tidal currents of the present model. It can be assumed that the sustaining rate of energy, which the internal currents draw from the tide-generating forces via the averaged currents, is almost completely lost by bottom friction. This assumption is strongly supported by the present result that the total rate of ocean eddy dissipation (ROED, Table

9) is zero within three significant figures. Thus, it is remarkable to find Munk's (1966; see also Wunsch, 1975, and Cartwright, 1977) famous estimate of $0.5Z10^{12}$ Watt for the rate of energy that the internal tidal currents receive and lose to sustain their comotion falling right into the center of the range $(0.41–0.60)\times 10^{12}$ Watt derived above for the rate of deep bottom friction work done by the fluctuating currents. In fact, even the (trivial) upper limit is safely below the extreme upper estimate of $0.7Z10^{12}$ Watt established by Wunsch (1975).

Finally, attention may be drawn to the computed kinetic and potential energies that are stored in the tidal motions. As was explained for the global tide data (RSTE-RBDW) above and C^{+}_{22} in the preceding section, one finds again the same numerical agreement between the potential energies PE = $1.07\cdot10^{17}$ Joule and $1.34\cdot10^{17}$ Joule computed, respectively, for the present model and for the Parke-Hendershott (1980) model. Unfortunately, no other energy data can be compared between the two tide models, because the Parke-Hendershott (1980: 388) model failed to allow computations of global data containing tidal velocity components. The present ocean tide model evolved through extensive computer experiments to determine physically realistic bottom friction and eddy dissipation laws in hydrodynamically defined ocean tidal equations by coherently integrating thousands of empirical tide data around the world. The complete solution of the final hydrodynamical equations of tidal motions yielded simultaneously realistic tidal elevation and velocity fields with a perfectly balanced energy budget in verifiable terms and with gratifying results in a broad range of practical and scientific applications.

Simple Model Improvements

In coastal waters some of the shortcomings of the M_2 ocean tide model (see preceding sections) can be immediately removed by preparing more detailed limited-area tide models on a locally refined grid system. Models of this sort have already been constructed by various researchers (Defant, 1961; Flather, 1976; Suendermann, 1977; Liu and Leendertse, 1979; Cartwright et al., 1980; Davis and Furnes, 1980; Godin, 1980; Pearson et al., 1980;

Prandle, 1980; Malone and Kuo, 1981; MacAyeal, 1982), especially for globally excluded or insufficiently resolved border seas. Where no refined models are available, a simple refinement may be accomplished by linear or higher-order interpolation of the listed 1° × 1° data and by using additional empirical data, say, from the huge collections of the British Admiralty (1977) and the International Hydrographic Bureau (1978). In such a refining process the hydrodynamically interpolated empirical tide data that are listed for the centers of the grid cells should be first returned as closely as possible to the original tide gauge locations. Specifically in boundary cells the empirical data should be moved from the cell centers to the centers of the corresponding land-boundary mesh segments. For small (unresolved) islands or near-shore gauge stations the tabulated empirical data should be shifted from the cell centers to the original stations. This relatively simple local procedure is strongly recommended where ocean tides suffer drastic distortions from rough bottom reliefs (Figures 1 and 2; Table 4). It is particularly significant in local studies of, say, gravity anomalies in near-shore areas (see, e.g., the preceding three sections and Sasao and Sato, 1981).

During the publication period of this paper, W. J. Pierson (see also Neumann and Pierson, 1966) communicated to the author that the M_2 tide possesses in its frequency neighborhood (M_2 Group) five minor partial tides of measurable strength, which are frequency-wise unseparable from M_2 in most experimental records of earth and ocean tides and of their gravitational effects. In fact, as can be seen from the Doodson numbers in Table 10, the side mode (1) alone contains 3.7% of the M_2 power and has a beat period of 18.61 yr relative to M_2 (the beat period corresponds to the frequency difference: $\sigma - \sigma_1$). Similarly, side modes (2) and (3) have beat periods of 1 yr, and side modes (4) and (5) have beat periods of 1/2 yr each relative to M_2. Together, all five side modes (1) to (5) contain 4.8% of the M_2 strength and may not be negligible in special applications (see, e.g., "Spherical Harmonic Coefficients of M_2 Ocean Tides" above).

Table 10
Leading harmonic equilibrium tides of M_2 group
(Neumann and Pierson, 1966; Cartwright and Edden, 1973)

Reference Symbol	*Doodson Number*	*K (cm)*	*σ (10^{-4}/sec)*	*χ (deg)*
M_2	*255.555*	*24.2322*	*1.405189026*	*$2h_o - 2s_o$*
1	255.545	0.9046	1.40508?056	$2h_o - 2s_o - N_o + 180$
2	254.556	0.0835	1.40319 57	$h_o - 2s_o + \Gamma_o + 180$
3	256.554	0.0739	1.407179995	$3h_o - 2s_o - \Gamma_o$
4	253.755	0.0728	1.401656984	$2p_o - 2s_o + 180$
5	257.555	0.0278	1.409171154	$4h_o - 2s_o$

K = amplitude of equilibrium partial tide.
σ = frequency of partial tide.
χ = astronomical argument of partial tide.
$(h_o, s_o, p_o, \Gamma_o, N_o)$ = mean longitudes of: sun, moon, lunar perigee, lunar ascending node (negative), and solar perigee at Greenwich midnight of day d, where:

$$h_o = 279.696\,68 + 36\,000.768\,925\,485T + 3.03 \cdot 10^{-4}\,T^2.$$

$$s_o = 270.434\,358 + 481\,267.883\,141\,37T - 0.001\,133T^2 + 1.9 \cdot 10^{-6}\,T^3.$$

$$p_o = 334.329\,653 + 4\,069.034\,032\,957\,5T - 0.010\,325T^2 - 1.2 \cdot 10^{-5}\,T^3.$$

$$N_o = -259.183275 + 1934.142008355T - 0.002078T^2 - 2 \cdot 10^{-6}\,T^3.$$

$$\Gamma_o = 281.22083 + 1.7191733100T + 0.000453T^2 + 3 \cdot 10^{-6}\,T^3.$$

and

$$T = [27\,392.500\,528 + 1.000\,000\,035\,6D]/36\,525.$$

$$D = d + 365(y - 1975) + \text{Int}[(y - 1973)/4].$$

d = day number of year (d = 1 for January 1).
$y \geq 1975$ = year number.
Int [x] = integral part of x.

For practical applications the combined equilibrium (η), earth (ζ^e), and ocean (ζ) tides of the M_2 group may be written (see Equations 1,2,3, and Table 10) in the respective superposed forms:

$$\tilde{\eta} = K\cos^2\phi\cos(\sigma t+2\lambda+\chi)+\sum_{i=1}^{5} K_i\cos^2\phi\cos(\sigma_i t+2\lambda+\chi_i)$$

$$\tilde{\zeta}^e \approx 0.612\tilde{\eta}$$

$$\tilde{\zeta} \approx \xi\cos(\sigma t-\delta+\chi)+\sum_{i=1}^{5}\xi_i\cos(\sigma_i t-\delta_i+\chi_i),$$

where approximately

$$\xi_i \approx \xi K_i/K \text{ and } \delta_i \approx \delta \quad (i = 1,2,3,4,5) \tag{10}$$

or in the lumped forms:

$$\tilde{\eta} = \beta(t)K\cos^2\phi\cos[\sigma t+2\lambda+\chi+\chi'(t)],$$

$$\tilde{\zeta}^e \approx 0.612\tilde{\zeta},$$

$$\tilde{\zeta} \sim \beta(t)\xi\cos]\sigma t-\delta+\chi+\chi'(t)],$$

where $\beta(t)$ and $\chi'(t)$ denote the "beat factor" and the "beat shift" of the lumped tides. Both β and χ' can be derived from the known equilibrium tide η in the superposed form (9a) (Dietrich, 1963; Neumann and Pierson, 1966). The somewhat involved functions contain the beat frequencies mentioned above and, hence, vary slowly with time. The 4.8% side-mode power translates into a $\pm 4.8\%$ variation of the beat factor and the lumped amplitude. Obviously, a variation of this magnitude could bring empirical and theoretical tidal comparisons closer together, provided theoretical data are applied in lumped form or, vice versa, beat effects are removed from empirical data. Fortunately, most ocean tide gauge records have been analyzed with due regard to beat modulations.

Due to the involved functions $\beta(t)$ and $\chi'(t)$ the simple superposed forms (9) with the approximations (10) may be more convenient in practical applications. Indeed, these approximations set all five ocean tide side modes directly proportional to the central M_2 ocean tide and require no extra (usually infeasible) amplitude and phase computations. The satisfactory validity of the approximations (10) were first found (Schwiderski, 1979b) to hold true even between the major ocean tidal components S_2 and K_2 (Dood-

son numbers 273.555 and 275.555), which have a beat period of 1/2 yr with a beat factor variation of ±27.2% (see Table 1). This may be verified by comparing the computed and empirical amplitudes and phases in the data charts of S_2 and K_2 (Schwiderski, 1983a,c).

The rather strong amplitude and phase variations with time of M_2 and other tidal constituents and of their corresponding gravitational effects have recently been verified experimentally by Baker and Alcock (1981) with a surprising emphasis. In addition to the beat effect of unresolved components, other mostly ignored sources were detected to cause even larger tidal variations. For example, daily and seasonal atmospheric fluctuations were identified to boost amplitude and phase variations of S_2 and K_1 ocean tides to an amazing 8% and 5° and even 30% and 15°, respectively. Clearly, distortions and retardations of this magnitude limit severely the accuracy and reliability of empirical data and must be considered in future analyses of any observed records of earth and ocean tides and of their gravitational effects.

Acknowledgments

The author wishes to thank the editor of this journal, Prof. N. K. Saxena, and his referees for inviting and encouraging the publication of this paper. Taking this opportunity, the author acknowledges with pleasure and thanks friendly and valuable communications that he received from Dr. C. C. Goad of the National Geodetic Survey/NOS/NOAA, Rockville, Maryland; Dr. P. Melchior, Director Observatoire Royal de Belgique, Brussels; and Prof. W. J. Pierson, Jr., of the City University of New York, New York. Many critical and stimulating suggestions were gratefully received from the author's colleagues, Dr. C. J. Cohen and Dr. B. Zondek. The astronomical arguments listed in the paper were supplied by Mr. W. J. Groeger. The involved computer programs were all prepared by Mr. L. T. Szeto in his competent and effective manner.

In private communications, important empirical tide data were gratefully received from: Mr. D. C. Simpson (1977), Messrs. S. K. Gill and D. L. Porter (1978), all at National Ocean Sur-

vey/NOAA, Rockville, Maryland; Prof. K. Wyrtki (1978) at University of Hawaii, Honolulu, Hawaii; Prof. B. D. Zetler (1978) at Scripps Institution of Oceanography, San Diego, California; Dr. D. E. Cartwright (1978) and Dr. D. Pugh (1979), both at Institute of Oceanographic Sciences, Bidston Observatory, United Kingdom. Numerous empirical tide data were taken from articles by: Defant (1961), Miyazaki et al. (1967), Nowroozi et al. (1969), Munk et al. (1970), Zahel (1970), Irish et al. (1971), Irish and Snodgrass (1972), Nowroozi (1972), Luther and Wunsch (1975), Mofjeld (1975), Pearson (1975), Zetler et al. (1975), Cartwright et al. (1979), Pugh (1979), and Gill and Porter (1980). Large empirical tide data collections were taken from the publications of the National Ocean Survey (1942), British Admiralty (1977), and the International Hydrographic Bureau (1978).

This project was supported by the Naval Surface Weapons Center's Independent Research Fund and by a grant from the National Geodetic Survey/National Ocean Survey/NOAA, Rockville, Maryland. It is the author's most pleasant obligation to acknowledge the sustained and generous sponsorship of Mr. O. F. Braxton, Head of the Strategic Systems Department; his Research Associate, Dr. R. J. Anderle; and Mr. C. W. Duke, Jr., Head of the Space and Surface Systems Division.

References

Accad, Y., and Pekeris, C. L. 1978. Solution of the Tidal Equations for the M_2 and S_2 Tides in the World Oceans from a Knowledge of the Tidal Potential Alone. *Phil. Trans. Roy. Soc.*, London, Ser. A, 290: 235.

Baker, T. F., and Alcock, G. A. 1981. On the Time Variation of Ocean Tides. *Proceedings of the Ninth International Symposium on Earth Tides*, Columbia University, New York, N.Y., August 17–22.

British Admiralty Tide Tables. 1977. Vols. 1, 2, and 3. London.

Cartwright, D. E. 1977. Ocean Tides. *Rep. Prog. Phys.*, 40: 665.

Cartwright, D. E., and Edden, A. C. 1973. Corrected Tables of Tidal Harmonics. *Geophys. J. R. Astr. Soc.*, 33: 253.

Cartwright, D. E., Zetter, B. D., and Hamon, B. V. 1979. Pelagic Tidal Constants. *IAPSO Publication Scientifique* No. 30.

Cartwright, D. E., Edden, A. C., Spencer, R., and Vassie, J. M. 1980. The Tides of the Northern Atlantic Ocean. *Phil. Trans., Roy. Soc.*, London, 298: 87.

Cazenave, A. S., and Daillet, S. 1977. The Starlette Satellite-Preliminary Results. Internat. *Report de Rech. Geod. Sp.*, Toulouse, France.

Cazenave, A. S., and Daillet, S. 1981. Lunar Tidal Acceleration From Earth Satellite Orbit Analysis. *J. Geophys. Res.*, 86B3: 1659.

Daillet, S. 1978. Determination par observation des trajectoires de satellites artificiels des ondes semi-diurnes de la maree oceanique. Application au calcul de l'acceleration seculaire de La Lune. Ann. *Geophys.*, 14: 79.

Davis, A. M., and Furnes, G. K. 1980. Observed and Computed M_2 Tidal Currents in the North Sea. *J. Phys. Oceanogr.*, 10: 237.

Defant, A. 1961. *Physical Oceanography*. Vol. II. New York: Pergamon Press.

Dietrich, G. 1963. *General Oceanography, an Introduction*. New York, London: Interscience Publishers, Div. John Wiley & Sons.

Estes, R. H. 1977. A Computer Software System For the Generation of Global Ocean Tides including Self-Gravitation and Crustal Loading Effects. Tech. Rep. X-920 77-82, Goddard Space Flight Center, Greenbelt, Marvland.

Estes, R. H. 1980. A Simulation of Global Ocean Tide Recovery Using Altimeter Data with Systematic Orbit Error. *Marine Geodesy*, 3: 75.

Farrell, W. E. 1972. Deformation of the Earth by Surface Loads. *Rev. Geophys. Space Phys.*, 10: 261.

Farrell, W. E. 1973. Earth Tides, Ocean Tides and Tidal Loading. Phil. Trans. Roy. Soc., London., Ser. A, 274: 253.

Farrell, W. E. 1979. Earth Tides. *Rev. Geophys. and Sp. Phys.*, 17: 1442.

Farrell, W. E., Berger, J., and Agnew, D. 1982. IDA Tides. Fourth Annual Conference on the NASA Geodynamics Program, January 26-29, Greenbelt, Maryland.

Felsentreger, T. L., Marsh, J. G., and Williamson, R. G. 1979. M_2 Ocean Tide Parameters and the Deceleration of the Moon's Mean Longitude from Satellite Orbit Data. *J. Geophy. Res.*, 84, B9: 4675.

Flather, R. A. 1976. A Tidal Model of the North-West European Continental Shelf. *Memo. Soc. Roy. des Sc. de Liege*, 6X: 141.

Gill, S. K., and Porter, D. L. 1980. Theoretical Offshore Tide Range Derived from a Simple Defant Tidal Model Compared With Observed Offshore Tides. *International Hydrographic Review*, Monaco, LVII: 155.

Goad, C. C. 1980a. Gravimetric Tidal Loading Computed From Integrated Green's Functions. *J. Geophysical Research*, 85, B5: 2679.

Goad, C. C. 1980b. The Computation of Tidal Loading Effects with Integrated Green's Functions. *Proceedings of the Second International Symposium on Problems Related to the Redefinition of North American Vertical Geodetic Networks*, May 26-30, Ottawa, Canada.

Goad, C. C., and Douglas, B. C. 1978. Lunar Tidal Acceleration Obtained from Satellite-Derived Ocean Tide Parameters. *J. Geophys. Res.*, 83: 2306.

Godin, G. 1980. Cotidal Charts for Canada. Manuscript Rep. Ser. No. 55, Marine Sc. and Inf. Directorate, Department of Fisheries and Oceans, Ottawa, Ontario.

Hendershott, M. C. 1972. The Effects of Solid Earth Deformation on Global Ocean Tides. *Geophys. J. R. Astr. Soc.*, 29: 389.

International Hydrographic Bureau. 1978. Tides, Harmonic Constants, Computer Tape. Monaco.

Irish, J. D., and Snodgrass, F. E. 1972. Australian-Antarctic Tides. Antarctic Res. Ser., Vol. 19, Antarctic Oceanology II: The Australian-New Zealand Sector, edited by D. E. Hayes, *AGU*, p. 101.

Irish, J. D., Munk, W. H., and Snodgrass, F. E. 1971. M_2 Amphidrome in the Northeast Pacific. *Geophys. Fluid Dyn.*, 2: 355.

Lambeck, K., Cazenave, A. S., and Balmino, G. 1974. Solid Earth and Ocean Tides estimated from Satellite Orbit Analysis. *Rev. Geophys. Sp. Phys.*, 12: 421.

Liu, S. K., and Leendertse, J. J. 1979. A Three-Dimensional Model for Estuaries and Coastal Seas: Volume VI, *Briston Bay Simulations. Techn. Rep.* R-2405-NOAA, Rand, Santa Monica, California.

Luther, D. S., and Wunsch, C. 1975. Tidal Charts of the Central Pacific Ocean. *J. Phys. Ocean*, 5: 227.

MacAyeal, D. R. 1982. A Numerical Simulation of the Ross Sea Tides. To be published in the *Journal of Geophysical Research.*

Malone, F. D., and Kuo, J. T. 1981. Semi-Implicit Finite Element Methods Applied to the Solution of the Shallow Water Equations. *J. Geophys. Res*, 86, C5: 4029.

Marchuk, G. I., and Kagan, B. A. 1977. Ocean Tides: Mathematical Models of Numerical Experiments. (In Russian). Gidrometeoizdat, Leningrad.

Marchuk, G. I., Gordeyev, R. G., Rivkind, V. Y., and Kagan, B. A. 1973. A Numerical Method for the Solution of Tidal Dynamics Equations and the Results of its Application. *J. Comput. Phys.*, 13: 15.

Marsh, J. G., Felsentreger, T. L., and Williamson, R. G. 1982. Estimation of Geodynamic and Geodetic Parameters from Satellite Laser Tracking Data. Fourth Annual Conference on the NASA Geodynamics Program, January 26–29, Greenbelt, Maryland.

Melchior, P., and DeBecker, M. 1982. A Discussion of the World-Wide Measurements of Tidal Gravity with Respect to Oceanic Interactions, Lithosphere Heterogeneities, Earth's Flattening and Inertial Forces. General Meeting of IAG, May 7–20, Tokyo, Japan.

Melchior, P., Moens, M., and Ducarme, B. 1980. Tidal Gravity Profiles 1973–1980. *Bulletin D'Observations: Marees Terestres,* Vol. IV, 5, Observatoire Royal de Belgique.

Melchior, P., Moens, M., Ducarme, B., and Van Ruymbeke, M. 1981. Tidal Loading Along a Profile Europe-East Africa-South Asia-Australia and the Pacific Ocean. Communications, Serie A. No. 61, Observatoire Royal de Belgique.

Miller, G. R. 1966. The Flux of Tidal Energy out of the Deep Oceans. *J. Geophys. Res.*, 71: 2485.

Miyazaki, M., Juronuma, S., and Inoue, T. 1967. Tidal Constants Along the Coast of Japan. *Oceanogr. Mag.*, 19: 13.

Mofjeld, H. O. 1975. Empirical Model for Tides in the Western North Atlantic Ocean. NOAA, TR-ERL 340-AOML 19, Boulder, Colorado.

Munk, W. H. 1966. Abyssal Recipes. *Deep-Sea. Res.*, 13: 707.

Munk, W. H., and Cartwright, D. E. 1966. Tidal Spectroscopy and Prediction. *Phil. Trans., Roy. Soc.*, London, Ser. A, 259: 533.

Munk, W. H., Snodgrass, F. E., and Winbush, M. 1970. Tides Offshore: Transition from California Coastal to Deep-Sea Waters. *Geophys. Fluid Dyn.*, 1: 161.

Munk, W. H., Zetter, B., Clark, J., Gill, S., Porter, D., Spiesberger, J., and Spindel, R. 1981. Tidal Effects on Long-Range Sound Transmission. *J. Geophys. Res.* 86, C7: 6399.

National Ocean Survey. 1942. Tidal Harmonic Constants. U.S. Coast and Geodetic Survey, Washington, D.C.

Neumann, G., and Pierson, W. J., Jr. 1966. *Principles of Physical Oceanography*. Englewood Cliffs, New Jersey: Prentice-Hall, Inc.

Nowroozi, A. A. 1972. Long-Term Measurements of Pelagic Tidal Height off the Coast of Northern California. *J. Geophys. Res.*, 77: 434.

Nowroozi, A. A., Kuo, J. T., and Ewing, M. 1969. Solid Earth and Oceanic Tides Recorded on the Ocean Floor of the Coast of Northern California. *J. Geophys. Res.*, 24: 605.

Parke, M. E., and Hendershott, M. C. 1980. M_2, S_2, K_1, Models of the Global Ocean Tides on an Elastic Earth. *Marine Geodesy*, 3: 379.

Pearson, C. A. 1975. Deep-Sea Tide Observations off the Southeastern United States. NOAA T. Memo. No. 17, Rockville, Maryland.

Pearson, C. A., Mofjeld, H. O., and Tripp, R. B. 1980. Tides of the Eastern Bering Sea Shelf. Contribution No. 431 from the NOAA/ERL Pacific Marine Environmental Laboratory, Seattle, Washington.

Pekeris, C. L. 1978. The Bodily Tide and the Yielding of the Earth Due to Tidal loading. *Geophys. J. Roy. Astr. Soc.*, 52: 471.

Pekeris, C. L., and Accad, Y. 1969. Solution of Laplace's Equation for the M_2 Tide in the World Oceans. *Phil. Trans. Roy. Soc.*, London, Ser. A, 265: 413.

Prandle, D. 1980. Co-Tidal Charts for the Southern North Sea. Deut. *Hydrogr. Zeitschr.*, 33: 68.

Proudman, J. 1952. *Dynamical Oceanography*. New York: Dover Publications, Inc.

Pugh, D. 1979. Sea Levels at Aldabra Atoll, Mombasa and Mahé, Western Equatorial Indian Ocean, Related to Tides, Meteorology, and Ocean Circulation. *Deep-Sea Res.*, 26A: 237.

Sasao, T., and Sato, T. 1981. Effects of the Oceanic Tides Upon the Astronomical Time and Latitude Observations. *Proceedings of the Ninth International Symposium on Earth Tides*, Columbia University, New York, N.Y., August 17-22.

Schwiderski, E. W. 1978a. Global Ocean Tides, Part I: A Detailed Hydrodynamical Interpolation Model. NSWC/DL TR-3866.

Schwiderski, E. W. 1978b. A Detailed Hydrodynamical Interpolation Model of

Worldwide Ocean Tides. Presented at the Int. Symp. on Interaction of Marine Geodesy and Ocean Dynamics, Miami, Florida, October 10-15.

Schwiderski, E. W. 1979a. NSWC Ocean Tide Program. Presented at the NASA SEASAT ALT/POD Calibration Workshop, Austin, Texas, June 11-15.

Schwiderski, E. W. 1979b. Detailed Ocean Tide Models of (N_2, M_2, S_2, K_2) and (K_1, P_1, O_1, Q_1), Including an Atlas of Tidal Charts and Maps. Presented at the XVIIth General Assembly of the International Union of Geodesy and Geophysics in Canberra, Australia, December 2-15.

Schwiderski, E. W. 1979c. Global Ocean Tides, Part II: The Semidiurnal Principal Lunar Tide (M_2), *Atlas of Tidal Charts and Maps.* NSWC TR 79-414.

Schwiderski, E. W. 1980a. Ocean Tides, Part I: Global Tidal Equations. *Marine Geodesy,* 3: 161.

Schwiderski, E. W. 1980b. Ocean Tides, Part II: A Hydrodynamical Interpolation Model. *Marine Geodesy,* 3: 219.

Schwiderski, E. W. 1980c. On Charting Global Ocean Tides. *Reviews of Geophysics and Space Physics,* 18: 243.

Schwiderski, E. W. 1981a. NSWC Global Ocean Tide Data (GOTD 1981) Tape. Magnetic Tape available at the Naval Surface Weapons Center, Dahlgren, Virginia 22448.

Schwiderski, E. W. 1981b. On the Application of the NSWC Ocean Tide Models to Interactions of Oceanic and Terrestrial Tides. *Proceedings of the Ninth International Symposium on Earth Tides,* Columbia University, New York N.Y., August 17-22.

Schwiderski, E. W. 1983a. Atlas of Ocean Tidal Charts and Maps, Part II: The Semidiurnal Principal Solar Tide S_2. (In preparation.)

Schwiderski, E. W. 1983b. Atlas of Ocean Tidal Charts and Maps, Part III: The Diurnal Luni-Solar Declination Tide K_1. (In preparation.)

Schwiderski, E. W. 1983c. Atlas of Ocean Tidal Charts and Maps, Part VII: The Semidiurnal Luni-Solar Declination Tide K_2. (In preparation.)

Schwiderski, E. W. 1983d. Atlas of Ocean Tidal Charts and Maps, Part XII: Synoptic Features of Semidiurnal, Diurnal and Long-Period Ocean Tides. (In preparation.)

Schwiderski, E. W. 1983e. Exact Expansions of Arctic Ocean Tides. (In preparation.)

Schwiderski, E. W., and Szeto, L. T. 1981a. The NSWC Global Ocean Tide Data Tape (GOTD), Its Features and Application, Random-Point Tide Program. *NSWC* TR 81-254.

Schwiderski, E. W., and Szeto L. T. 1981b. On Computing Instantaneous Geocentric Tides Along Satellite Tracks, the NSWC STT Program. *NSWC* TR 81-264.

Suendermann, J. 1977. The Semidiurnal Principal Lunar Tide M_2 in the Bering Sea. *Deut. Hydrogr. Zeitschr.* 30: 91.

Taylor, G. I. 1918. Tidal Friction in the Irish Sea. *Phil. Trans. Roy. Soc.*, London, A, 230: 1.

Van Ruymbeke, M., Ducarme, B., and DeBecker, M. 1981. An Attempt to Model the Tidal Triggering of Earthquakes. *Ninth International Symposium on Earth Tides*, Columbia University, New York, N.Y., August 17-22.

Wahr, J. M., and Sasao, T. 1981a. A Diurnal Resonance in the Ocean Tide and in the Earth's Load Response Due to the Resonant Free Core Nutation. *Geophys. J. Res. Astr. Soc.*, 64: 747.

Wahr, J. M., and Sasao, T. 1981b. A Nearly Diurnal Resonance in Ocean Load Tide. *Proceedings of the Ninth International Symposium on Earth Tides*, Columbia University, New York, N.Y., August 17-22.

West, G. B. 1981. SEASAT Satellite Radar Altimetry Data Processing System. *NSWC* TR 81-234.

Wunsch, C. 1975. Internal Tides in the Ocean. *Rev. Geophys. Sp. Phys.*, 13: 167.

Yoder, C. F. 1982. Spherical Harmonic Decomposition of M. E. Parke's Ocean Tidal Models. *Engineering Memorandum* 335-30, Jet Propulsion Laboratory, Pasadena, California.

Zahel, W. 1970. Die Reproduktion Gezeitenbedingter Bewegungsvorgange im Weltozean Mittels des Hydrodynamisch-Numerischen Verfahrens. *Mitteilungen des Inst. f. Meereskunde der Univ. Hamburg.* XVII.

Zahel, W. 1977. The Influence of Solid Earth Deformations on Semidiurnal and Diurnal Oceanic Tides. In: *Tidal Friction and Earth's Rotation*, P. Brosche and J. Suendermann, ed. New York: Springer, p. 98.

Zetler, B. D., Munk, W. H., Mofjeld, H. O., Brown, W., and Dormer, F. 1975. MODE Tides. *J. Phys. Oceanogr.*, 5: 430.

Appendix A

Atlas of 1° × 1° M_2 Ocean Tide Amplitude and Phase Charts for 42° × 71° Areas

Guide to Tidal Charts

M = m:longitude number
N = n:colatitude number
λ_m = (m − 0.5)°:geographical longitude East
θ_n = (n − 0.5)°:geographical colatitude
$\xi_{m,n}$ = $\xi(\lambda_m,\theta_n)$:amplitude (in cm)
$\delta_{m,n}$ = $\delta(\lambda_m,\theta_n)$:Greenwich phases (in deg.;30° ≈ 1h)
⊗ = Amphidromic points
= Subbars mark empirical input data at shore stations
[= Subbrackets mark empirical input data at nearshore deep-sea stations

~ = Subtildes mark approximately distant offshore deep-sea stations with excluded empirical tide data listed in Tables 2 and 3

Note: The tidal charts are printed on microfiche, which can be obtained from the author. Printouts may be found in Schwiderski (1979c).

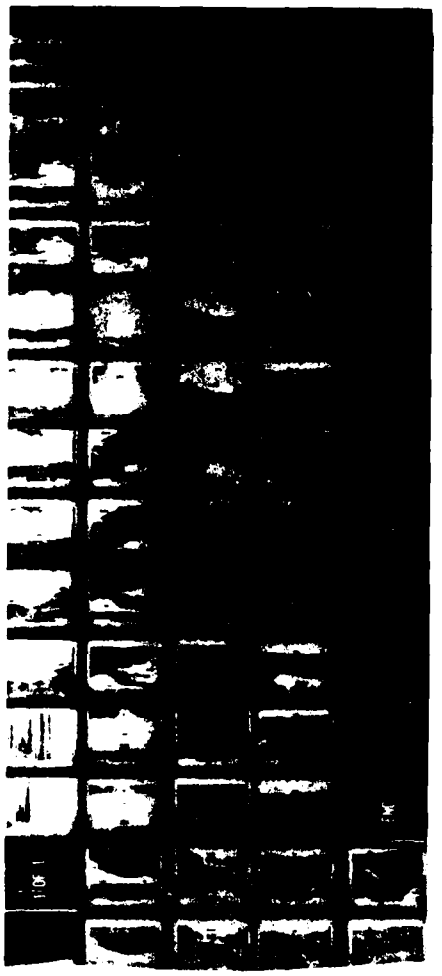

Appendix B

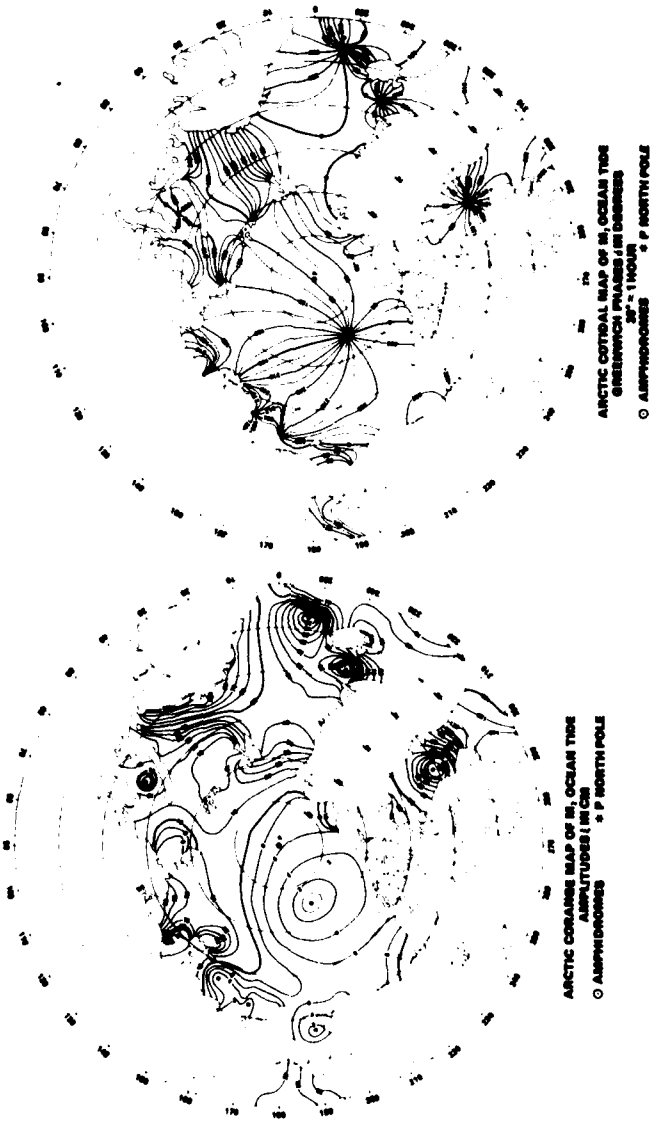

Figures 1-2. Atlas of Corange and Cotidal Maps of the M_2 Ocean Tide.

Figure 3. Amplitudes ξ of corange lines in centimeters.

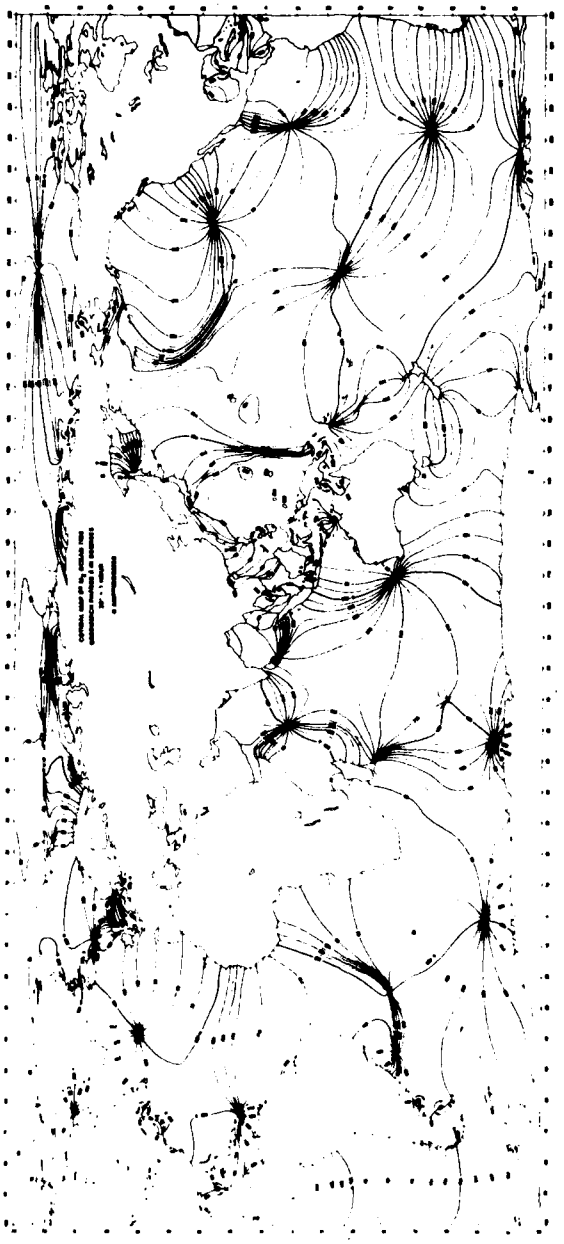

Figure 4. Greenwich phases δ of cotidal lines in degrees, where 30° ≈ 1 hour.